Journal of Medicinal Chemistry

Article

pubs.acs.org/jmc

Ligand-Based Design of a Potent and Selective Inhibitor of Cytochrome P450 2C19

Robert S. Foti,[†] Dan A. Rock,[†] Xiaogang Han,[‡] Robert A. Flowers, II,[§] Larry C. Wienkers,[†] and Jan L. Wahlstrom*[,†]

[†]Pharmacokinetics and Drug Metabolism, Amgen Inc., Seattle, Washington 98119, United States

[‡]Pharmacokinetics and Drug Metabolism Biomarkers, Pfizer, Inc., Groton, Connecticut 06340, United States

[§]Department of Chemistry, Lehigh University, Bethlehem, Pennsylvania 18015, United States

ABSTRACT: A series of omeprazole-based analogues was synthesized and assessed for inhibitory activity against CYP2C19. The data was used to build a CYP2C19 inhibition pharmacophore model for the series. The model was employed to design additional analogues with inhibitory potency against CYP2C19. Upon identifying inhibitors of CYP2C19, ligand-based design shifted to attenuating the rapid clearance observed for many of the inhibitors. While most analogues underwent metabolism on their aliphatic side chain, metabolite identification indicated that for analogues such as compound **30** which contain a heterocycle adjacent to the sulfur moiety, metabolism primarily occurred on the benzimidazole moiety. Compound **30** exhibited improved metabolic stability (Cl_{int} = 12.4 mL/min/nmol) and was selective in regard to inhibition of CYP2C19-catalyzed (*S*)-mephenytoin hydroxylation in human liver microsomes. Finally, representative compounds were docked into a homology model of CYP2C19 in an effort to understand the enzyme−ligand interactions that may lead to favorable inhibition or metabolism properties.

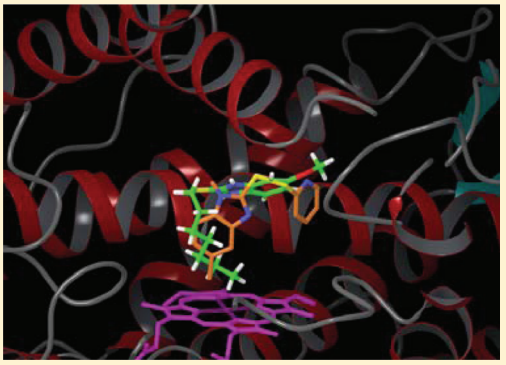

INTRODUCTION

The cytochromes P450 (P450) are a superfamily of heme-containing proteins that are capable of catalyzing the oxidative metabolism of a wide range of substrates. Common metabolic pathways that occur through P450 catalysis include hydroxylation, heteroatom oxidation or dealkylation, and aromatic oxidation.[1] Nearly 60 human P450s have been identified, with the major isoforms involved in drug metabolism being CYP1A2, CYP2A6, CYP2B6, CYP2C8, CYP2C9, CYP2C19, CYP2D6, CYP2E1, CYP3A4, and CYP3A5.[2] In addition to being involved in the metabolism of a wide array of drugs, P450 enzymes can also be the target of clinically relevant drug interactions or can form bioreactive metabolites that can have toxicological consequences.[3] Multiple examples exist within the literature describing the synthesis of potent and selective P450 inhibitors in order to invoke a pharmacological response or as diagnostic tools to assess the role of a given P450 isoform in a test compound's metabolism or drug interaction potential. Recent medicinal chemistry efforts have identified potent and selective inhibitors of CYP1B1, CYP2A6, and CYP26 through a combination of traditional synthesis and computational tools.[4−6]

CYP2C19 is a polymorphic enzyme that is localized in the liver (approximately 5% of hepatic P450) and intestine (less than 3% of intestinal P450).[7,8] The enzyme is inducible by rifampicin, phenobarbital, and dexamethasone.[9,10] The typical reactions used to monitor CYP2C19 activity include (*S*)-mephenytoin 4′-hydroxylation, omeprazole 5-hydroxylation, and fluoxetine *O*-demethylation with the choice of substrate playing an important role in the observed CYP2C19 activities and drug interaction profiles.[11] Drugs that are metabolized in vivo by CYP2C19 include anticonvulsants such as phenytoin, psychotropic drugs such as imipramine and diazepam, and the proton pump inhibitors omeprazole, lansoprazole, and rabeprazole.[12]

Proton pump inhibitors such as omeprazole block the release of gastric acid through inhibition of the H^+/K^+-ATPase pump in gastric parietal cells.[13] They are widely used to treat gastresophageal reflux disease (GERD) and Zollinger−Ellison syndrome.[14,15] The substituted benzimidazole sulfoxides are metabolized by a number of P450s, including CYP2C19, CYP3A4, and CYP2D6.[16,17] The various proton pump inhibitors have gained attention from a drug metabolism standpoint because of their potential to cause drug interactions both in vitro and in vivo. In human liver microsomes, omeprazole and lansoprazole have K_i values of approximately 3 μM against CYP2C19.[18] In vivo, omeprazole has been shown to have drug interactions with diazepam[19,20] and phenprocoumon.[21] The combination of the CYP2C19 metabolism and inhibition profiles of proton pump inhibitors such as omeprazole makes the class of compounds a useful tool to study both the substrate selectivity and active site characteristics of CYP2C19.

An inherent difficulty in optimizing the properties of P450 ligands is the simultaneous interplay of catalysis and inhibition. Unlike the development of a series of inhibitors against a therapeutic target where target potency and metabolic stability

Received: October 7, 2011
Published: January 12, 2012

   dx.doi.org/10.1021/jm201346g | *J. Med. Chem.* 2012, 55, 1205−1214

are assessed in discrete in vitro systems, compounds designed to inhibit a given P450 enzyme may be subject to metabolism by the same enzyme. In addition, the relationship between inhibition and metabolism may be series dependent. For example, a positive correlation between intrinsic clearance and inhibition potency has been noted for a series of quinoline-4-carboxamide compounds with CYP3A4, potentially due to their ability to type II bind to the here iron.[22,23] Conversely, for a series of HIV protease inhibitors, compounds with a lower intrinsic clearance were able to more potently inhibit CYP3A4.[24] Few examples exist of both catalytic and inhibitory models applied to the same set of compounds, most likely due to the complexities added by metabolism by multiple enzymes or at different sites on a molecule.[25]

The aim of this study was to design and synthesize a potent and selective inhibitor of CYP2C19 based on a series of omeprazole-based analogues. An initial set of 26 diverse structural omeprazole analogues was synthesized and assessed for inhibition of CYP2C19 (K_i). The data was subsequently used to populate pharmacophore-based models. Information gained from the pharmacophore models was used to direct the synthesis of additional analogues within the series. Upon identification of potent inhibitors of CYP2C19, the aim of the study shifted toward improving metabolic stability within the series. To this end, compounds were assessed for rates and sites of metabolism by CYP2C19. Both ligand- and active-site modeling were incorporated in order to more fully understand the chemical properties that confer both metabolism by and inhibition of CYP2C19. Finally, the interplay of metabolism and inhibition was examined in order to identify a highly potent and metabolically stable inhibitor of CYP2C19.

RESULTS

Assessment of CYP2C19 Inhibition. A series of omeprazole analogues was synthesized as depicted in Figure 1. The initial set of 26 omeprazole-based analogues was assessed for inhibition of CYP2C19-catalyzed 3-*O*-methylfluorescein metabolism. Prior to conducting the inhibition assay, a K_m was determined for the formation of fluorescein from 3-*O*-methylfluorescein in recombinant CYP2C19 (1.18 ± 0.06 μM) using reaction conditions that were previously determined to be linear with respect to time and protein concentration. IC_{50} values were obtained for each compound and used to determine the range of inhibitor concentrations for the K_i assay. Following the 5 min incubation, K_i values ranged from 0.04 μM (compound **19**) to >50 μM (compound **11** and **20**; Table 2).

A feature-based pharmacophore model was generated using the inhibition data obtained from the K_i assay. The data was fit to a three, four, five, or six feature model. In all cases, the hydrophobic regions (H) of the compound set represented a key feature of the model. In addition to hydrophobicity, the aromatic rings (R) of the benzimidazole moiety were also taken into account (Figure 2). For the three feature (HHR) and four feature (HHRR) pharmacophore models, the best fit was obtained when using three partial-least squared factors. When generating the pharmacophore models with five (ADHHR) or six (DHHHRR) features, the hydrogen bond accepting (A) and hydrogen bond donating (D) characteristics of the benzimidazole nitrogens were taken into account. The best overall fit from the pharmacophore models was obtained from the five feature ADHHR model (r^2 = 0.958, q^2 = 0.607, RMSE = 0.603). The features for this model corresponded to the hydrogen bond accepting (A) and donating (D) features of the benzimidazole nitrogens, the hydrophobicity of the side chains off of the sulfur atom (H), the side chain off of the benzimidazole moiety (H), and the aromaticity of the benzimidazole rings (R).

Table 1. Omeprazole-Like Inhibitors of CYP2C19

	R1	R2		R1	R2
1			17		
2			18		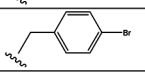
3			19		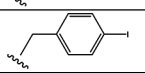
4			20		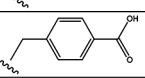
5			21		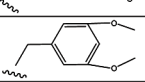
6			22		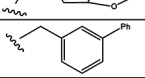
7			23		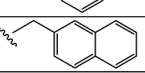
8			24		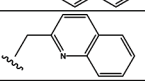
9			25		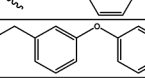
10			26		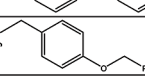
11			27		
12			28		
13			29		
14			30		
15			31		
16			32		

Figure 1. General synthetic route for the omeprazole-based analogues.

Following pharmacophore analysis, the series of omeprazole analogues was expanded to include a pyridine moiety linked to the mercapto-benzimidazole group at the R2 position with varying side-chains at R1. Upon synthesis of the heterocycle-containing compounds (compounds **27**−**32**), an increase in the observed potency was noted (compound **30**, K_i = 0.02 μM).

To assess the selectivity of the omeprazole-based analogues for CYP2C19, inhibition assays were repeated in human liver microsomes with selective probe substrates. Similar inhibition parameters (r^2 = 0.86) were observed for compounds that were active in both the recombinant system utilizing 3-*O*-methylfluorescein as the probe substrate or human liver microsomes which utilized (*S*)-mephenytoin as the probe substrate. Two of the most potent CYP2C19 inhibitors, compounds **15** and **30**, were 37- and 66-fold selective, respectively, for CYP2C19 in human liver microsomes as compared to the next most potently inhibited P450 isoform (CYP1A2 for both

dx.doi.org/10.1021/jm201346g | J. Med. Chem. 2012, 55, 1205−1214

Table 2. LogD$_{(pH=7.4)}$, K_i, and Intrinsic Clearance Values for Omeprazole-Based Analogues

compd	LogD (pH = 7.4)	CYP2C19 K_i (μM)	CYP2C19 Cl_{int} (mL/min/nmol P450)
1	2.92	42.5	0.44
2	3.45	4.79	2.77
3	3.98	0.75	8.00
4	4.51	0.06	23.39
5	5.05	0.07	29.13
6	5.58	0.05	24.07
7	3.8	0.06	8.61
8	4.15	1.00	5.57
9	3.29	1.94	2.19
10	4.98	0.14	22.55
11	1.98	50.0	<0.43
12	−0.34	40.8	<0.43
13	4.17	1.10	<0.43
14	4.63	0.13	24.80
15	5.51	0.04	20.98
16	5.86	0.20	28.53
17	4.76	0.10	26.08
18	4.94	0.07	25.66
19	5.2	0.04	19.67
20	0.95	50.0	0.44
21	3.88	0.07	20.66
22	5.92	0.07	11.62
23	5.4	0.06	34.51
24	4.03	0.85	<0.43
25	6.16	0.05	19.02
26	5.74	0.31	15.96
27	2.67	2.43	1.69
28	3.21	10.9	1.55
29	2.76	0.05	6.02
30	3.22	0.02	12.29
31	2.85	3.20	2.39
32	1.47	9.90	<0.43

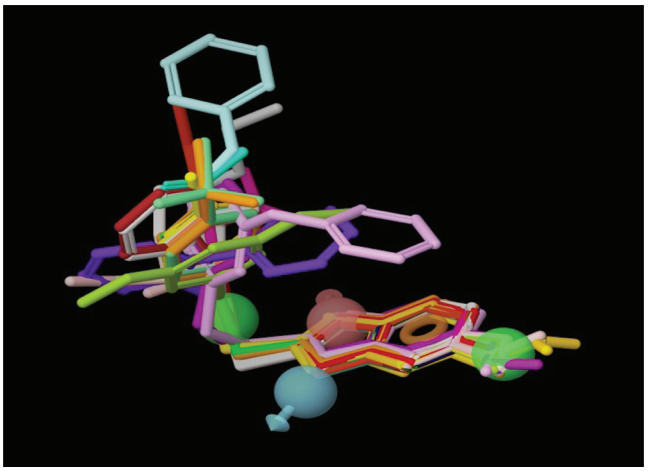

Figure 2. CYP2C19 inhibition pharmacophore model for the omeprazole-based analogues. The features for this five-feature model corresponded to the hydrogen bond accepting (blue) and donating (pink) features of the benzimidazole nitrogens, the hydrophobicity of the side chains off of the sulfur atom and the benzimidazole moiety (green), and the aromaticity of the benzimidazole rings (orange).

compounds). In general, inhibitor selectivity for CYP2C19 decreased as less potent CYP2C19 inhibitors were evaluated (Table 3).

Assessment of CYP2C19 Metabolism. Intrinsic clearance of each of the analogues was determined in both recombinant CYP2C19 and human liver microsomes. In general, the longer chain aliphatic analogues and substituted phenyl analogues were cleared the most rapidly (Tables 2 and 3). Hydroxyl and carboxylic acid analogues demonstrated the greatest degree of stability in both systems. Heterocyclic analogues were moderately stable in both systems (rCYP2C19 Cl_{int}, 0.43−12.3 mL/min/nmol; HLM Cl_{int}, 57.8−579.9 μL/min/mg).

A feature-based pharmacophore model was also generated using the intrinsic clearance values for the series of compounds (Figure 3). For the intrinsic clearance pharmacophore model, a minimum of five features (AADHR) with three partial least squared factors predicted intrinsic clearance values within an acceptable range (r^2 = 0.857; q^2 = 0.603; RMSE = 0.378). Both r^2 and q^2 values decreased significantly when the model was generated using only one or two partial least squared factors. For the metabolism pharmacophore model, the five features corresponded to the hydrogen bond accepting properties of one of the benzimidazole nitrogens (A) as well as the oxygen atom of the benzimidazole methoxy moiety (A), the hydrogen bond donating properties of the second benzimidazole nitrogen (D), the hydrophobicity of the side chains off of the sulfur atom (H), and the aromaticity of the benzimidazole rings (R).

Correlation of CYP2C19 Inhibitory Potency and Metabolic Stability With Physicochemical Properties. Physical properties for each of the 32 analogues were calculated using ChemDraw Ultra 9.0 (CambridgeSoft, Cambridge, MA) or a proprietary data analysis prediction software package. Inhibition potency values showed the best correlation with hydrophobic descriptors such as $LogD_{7.4}$. Plotting inhibition and intrinsic clearance values versus $LogD_{7.4}$ gave r^2 values of 0.78 and 0.64, respectively. The most potent inhibition values were observed for compounds with a $LogD_{7.4}$ greater than 4. In general, the most potent inhibitors were also the most rapidly cleared in recombinant CYP2C19 (Figure 4). Plotting K_i values determined in rCYP2C19 against intrinsic clearance values in the same system resulted in an r^2 value of 0.87.

Metabolite Identification. To determine the primary sites of metabolism for the omeprazole-based series, qualitative metabolite identification experiments were conducted on representative aliphatic/phenyl and heterocycle compounds. For the compounds that had an aliphatic side chain or phenyl moiety, the primary site of metabolism was on the hydrophobic side chain adjacent to the sulfur of the 2-mercapto-5-methoxybenzimidazole core structure. For compounds **3**, **5**, and **6**, monohydroxylation on the alkyl chain was the major route of metabolism (Figure 5). Fragmentation patterns from product ion scans indicated an increase of 16 amu to each of the alkyl chains, although the fragmentation was not specific enough to assign the hydroxyl group to a specific carbon on the chain. Synthesis of metabolite standards further indicated that metabolism was primarily occurring at the ω-1 carbon of the alkyl chain (data not shown). The primary metabolites of compound **7** (isopropyl) and compound **8** (*t*-butyl) were determined to be hydroxylation of one of the terminal carbons of the alkyl chain. Compounds **10** (cyclohexyl), **14** (*p*-tolyl), and **15** (*p*-cumyl) all showed a monohydroxylation on the respective cyclic ring as the major metabolite in recombinant CYP2C19. As with the alkyl side chains, the mass spectral fragmentation patterns did not allow for the specific site of metabolism on the cyclohexyl or aromatic rings to be elucidated. Minor routes of metabolism included hydroxylation

dx.doi.org/10.1021/jm201346g | J. Med. Chem. 2012, 55, 1205−1214

Table 3. IC_{50} and Intrinsic Clearance Values for Omeprazole-Based Analogues in Human Liver Microsomes

	IC_{50}, μM (HLM)								HLM		selectivity	
compd	1A2	2B6	2C8	2C9	2C19	2D6	2E1	3A4mdz	$T_{1/2}$	Cl_{int}, app		
1	2.34	5.1	6.97	50	50	4.93	50	50	14.0	493.6		
2	0.93	50.0	3.12	35.8	50	1.94	50	27.1	9.6	724.1		
3	0.71	50.0	33.7	39.9	50	2.63	50	50	8.4	823.0		
4	0.44	10.5	9.64	9.18	50	19.4	50	26.3	3.7	1852.9		
5	0.39	15.4	2.42	2.92	6.25	2.61	50	5.33	3.8	1843.1		
6	0.79	14.8	50	4.57	0.21	5.33	50	15.7	2.6	2665.4	3.8	CYP1A2
7	1.02	50.0	31.9	32.7	50	11.6	50	50	10.7	650.1		
8	49.9	16.6	50	21.2	14.1	50	50	50	59.3	116.9	1.2	CYP2B6
9	0.95	50.0	50	22.1	50	29.4	50	16.4	12.9	538.0		
10	2.67	21.4	5.11	4.41	5.91	50	50	6.23	9.3	744.4		
11	8.08	5.5	5.65	50	50	4.17	50	5.49	37.4	185.3		
12	50	28.8	50	50.0	50.0	50	50	50.0 >	120	<57.8		
13	ND	50.0	50	9.73	7.8	0.12	50	0.08 >	120	<57.8		
14	1.39	17.7	3.32	6.73	3.7	4.28	50	8.86	6.1	1141.7		
15	1.48	14.4	50	3.42	0.04	2.05	50	8.34	5.8	1194.8	37.0	CYP1A2
16	50	50.0	0.97	2.54	7.2	1.36	50	12.3	16.5	420.5		
17	0.95	3.6	1.44	5.98	7.1	1.23	50	4.86	4.4	1560.8		
18	0.81	9.6	1.87	3.25	0.78	0.09	50	4.23	4.2	1669.9		
19	1.81	4.4	3.87	5.15	0.12	0.41	50	4.91	85.7	80.9	3.4	CYP2D6
20	50	50.0	50	50.0	50.0	50	50	50.0	8.06	859.8		
21	10.69	19.9	3.35	2.32	50	9.12	50	0.72	12.8	543.5		
22	0.67	1.1	0.25	0.82	2.2	0.02	50	1.87	1.8	3893.3		
23	1.34	12.6	0.51	2.27	50	2.73	50	3.11	11.4	608.4		
24	0.73	15.5	3.49	6.18	50	10.5	50	2.81	4.92	1408.5		
25	0.63	2.0	50	0.96	0.07	1.5	50	2.49	5.12	1353.5	9.0	CYP1A2
26	>50	50.0	0.68	0.88	50	0.12	50	3.56	16.3	424.4		
27	8.56	50.0	50	0.55	50	13.15	50	4.01	26.53	261.2		
28	50	9.9	50	24.2	7.6	50	50	0.4	20.2	343.1		
29	12.94	24.0	4.78	50	50	8.79	50	3.75 >	120	<57.8		
30	3.29	50.0	50	50	0.05	50	50	3.61	31.3	221.4	65.8	CYP1A2
31	50	21.8	50	22.3	28.5	50	50	10.7	16.1	430.4		
32	50	8.4	0.99	6.97	50	2.17	50	0.52	11.95	579.9		

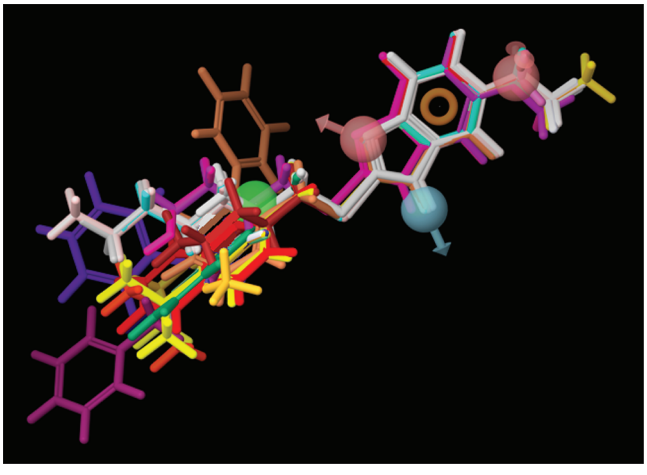

Figure 3. CYP2C19 metabolism pharmacophore model for the omeprazole-based analogues. The five features for the metabolism pharmacophore model corresponded to the hydrogen bond accepting properties of a benzimidazole nitrogen and the oxygen atom of the benzimidazole methoxy moiety (pink), the hydrogen bond donating properties of the second benzimidazole nitrogen (blue), the hydrophobicity of the side chains off of the sulfur atom (green), and the aromaticity of the benzimidazole rings (orange).

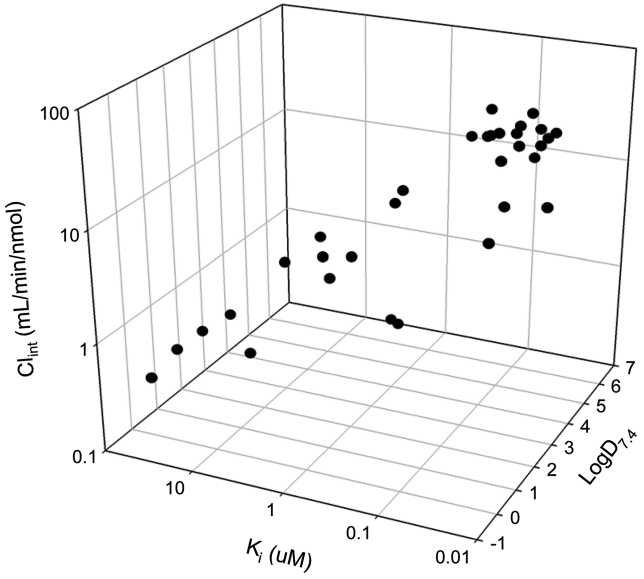

Figure 4. Three-dimensional correlation between inhibition potency (K_i), intrinsic clearance (Cl_{int}), and $LogD_{7.4}$. Calculated r^2 values were 0.78 (K_i versus $LogD_{7.4}$), 0.64 (Cl_{int} versus $LogD_{7.4}$), and 0.87 (K_i versus Cl_{int}).

of the benzimidazole moiety and *O*-demethylation at the 5-methoxy position.

When heterocyclic pyridine analogues attached to either a 2-mercapto-5-methoxybenzimidazole or 2-mercapto-5-methyl-

dx.doi.org/10.1021/jm201346g | *J. Med. Chem.* 2012, 55, 1205–1214

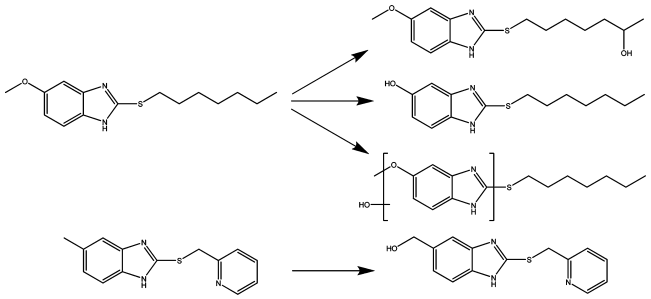

Figure 5. Identification of the primary sites of metabolism for this series of compounds. Compounds with a methoxy group at the 5-position of the benzimidazole ring and an aliphatic chain off of the sulfur were oxidatively metabolized at the ω-1 carbon of the aliphatic side chain, while compounds lacking the methoxy group and containing a heterocyclic ring off of the sulfur atom were primarily metabolized on the substituent at the 5-position of the benzimidazole ring.

benzimidazole core were assessed for metabolite formation in recombinant CYP2C19, the major routes of metabolism were observed to be a combination of hydroxylation on the benzimidazole moiety and *O*-demethylation (compound **27**) or hydroxylation on the 5-methyl substituent of the benzimidazole core (compound **30**). Only minimal amounts of sulfoxide or sulfone formation were observed for any of the compounds noted above.

CYP2C19 Active Site Docking. To evaluate the active site docking poses for CYP2C19 ligand interactions, a homology model of CYP2C19 was built and compounds **6** and **30** docked in the active site. Compound **6** docked in the active site of CYP2C19 with the heptyl side chain oriented toward the heme. The ω-1 carbon was located approximately 3.11 Å from the heme iron. Compound **30** docked in the opposite orientation, with the 5-methyl substituent of the benzimidazole core oriented toward the heme at a distance of 3.07 Å. The pyridine nitrogen of compound **30** occupied a similar space in the active site of CYP2C19 as the 5-methoxy moiety of compound **6**. In addition, both compounds were located within 2.00 Å of the CYP2C19 active site residues Val113, Val208, Glu300, Leu366, and Ala477. Additional interactions (within 3.00 Å) included Phe114, Ile205, Ser209, Thr301, Thr304, Ile362, Phe476, and Val479 (Figure 6).

DISCUSSION

Computational modeling of P450−ligand interactions has gained an increased amount of attention in recent years. Within this area of research, CYP2C19 has been the focus of a number of computational models aimed at predicting metabolism, structure−activity relationships, and the drug interaction potential for a given series of compounds. Examples include a series of benzbromarone-based analogues that was used to assess the effects of substrate charge and functional groups on affinity and metabolism,[26] the use of a GRID/CPCA (consensus principal component analysis) approach to compare the selectivity of CYP2C19 to CYP2C8, CYP2C9, and CYP2C18,[27] and a homology model/active site docking study to evaluate the metabolism of the sulfonylurea compound gliclazide.[28]

The most potent CYP2C19 inhibitors identified to date include (+)-*N*-3-benzylnirvanol, (−)-*N*-3-benzylphenobarbital, and 3,5″-dimethyl-4″-hydroxybenzbromarone, with K_i values ranging from 33 nM for the benzbromarone analogue to 250 nM

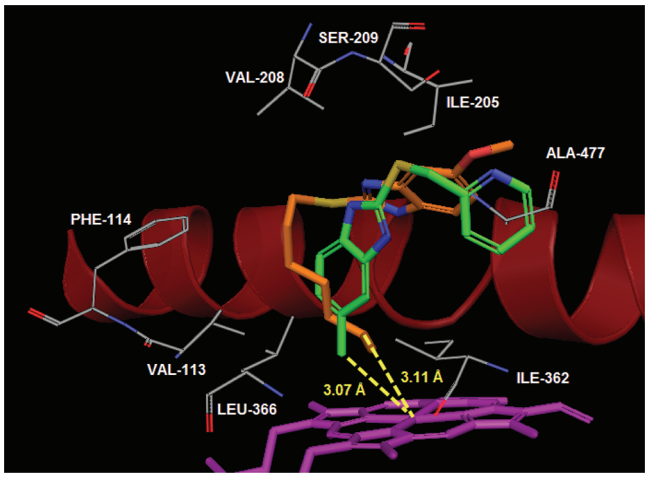

Figure 6. Active-site docking of compounds **6** (green) and **30** (orange) into a homology model of CYP2C19 (I-helix shown in red). Primary sites of metabolism were located approximately 3 Å from the heme iron, with the 5-methoxy group of compound **6** and the pyridine nitrogen of compound **30** occupying a similar space in the active site within approximately 2 Å of Ala477.

for (+)-*N*-3-benzylnirvanol.[26,29] Thus, the primary aim of this study was achieved in that the current set of compounds equals or surpasses these known inhibitors with respect to inhibitory potency against CYP2C19, with 14 of 32 compounds having K_i values equal to or less than 100 nM. Compound **30**, the 2-mercapto-5-methylbenzimidazole pyridine analogue, was the most potent compound synthesized, with a K_i value of 20 nM. While the range of inhibition values for the omeprazole-based analogues is comparable to what has been observed for the benzylnirvanol, benzylphenobarbital, and benzbromarone data sets, a striking difference between the compounds is the metabolic lability of the omeprazole-based compounds as compared to the other chemotypes.

While a significant amount of attention has been placed on using reaction conditions that avoid the depletion of the probe substrate in enzyme activity assays,[30] the stability of the test compound being assessed for inhibition is often neglected, except under conditions where inhibitory metabolites are suspected. For example, *N*-desmethyldiltiazem and *N*,*N*-didesmethyldiltiazem are both more potent inhibitors of CYP3A4 than diltiazem.[31] Conversely, *O*-desmethyldiltiazem was shown to have no inhibitory potential against CYP3A4. The compounds in this data set appear to be rapidly converted by CYP2C19 to metabolites with a decreased inhibitory affinity for the enzyme. This was observed by a decrease in the observed K_i values when enzyme activity was evaluated after a 5 min coincubation of probe substrate and inhibitor as compared to a 20 min coincubation (data not shown). In addition, compounds such as **11**, **12**, and **20** that contained either hydroxyl or carboxylic acid moieties showed no inhibitory potential against CYP2C19, suggesting a detrimental effect of polar groups on the affinity of the compounds for CYP2C19 and corroborating the importance of the hydrophobicity incorporated into both pharmacophore models. In light of this finding, it is quite likely that the hydroxylated metabolites of this series of analogues also have a decreased inhibitory potential for CYP2C19. Thus, for those compounds which were rapidly metabolized, calculating a K_i in human liver microsomes on a time scale consistent with the ability to measure an adequate amount of

dx.doi.org/10.1021/jm201346g | J. Med. Chem. 2012, 55, 1205−1214

(*S*)-mephenytoin hydroxylation may be difficult, as the actual concentration of inhibitor in the incubation will be much less than the original concentration added. Furthermore, if the actual amount of inhibitor is depleted to a point where it is equal to or less than the concentration of enzyme in the incubation, a percentage of the inhibitor will exist in equilibrium as the enzyme−inhibitor complex. The resulting deviation from starting conditions can result in an incorrect assessment of the inhibitor's potency.[32] A similar underestimation of the observed K_i or K_d has been reported for assays carried out using small volumes with an excess amount of enzyme.[33] In the previous case, however, the depletion of inhibitory ligand was caused by binding to a receptor that is in excess compared to the ligand.

When the metabolism and inhibition data were probed for physicochemical trends, the greatest correlation for both sets was versus the $LogD_{7.4}$ values for the compound set. Other descriptors of lipophilicity that showed a good correlation with the metabolism and inhibition values were cLogP, $LogD_{4.0}$, $LogD_{6.5}$ as well as the number of hydrogen bond donors. It has been previously reported that lipophilicity is an important factor in determining the potency of a set of CYP2C19 inhibitors.[34] More specifically, the lipophilic properties at the N-3 position of a series of phenytoin, nirvanol, or phenobarbital analogues were shown to drive the inhibitory potency of the compounds against both CYP2C9 and CYP2C19.[35]

To explore the structure−activity relationships for a given set of compounds, pharmacophore and docking/homology modeling are often utilized. The premise behind pharmacophore modeling is the superimposition of structural analogues with structural features including hydrogen bond acceptors or donors and π-stacking aromatic groups that may interact with the enzyme active site. Pharmacophore models can then be more fully incorporated as a useful descriptor in quantitative structure−activity modeling.[36−38] While less prevalent than inhibition modeling, recent attempts have also been made to model the metabolic clearance of compounds by P450 enzymes.[39] The development of both inhibition and metabolism pharmacophore models was achieved for the current set of compounds. We have successfully developed both an inhibition (r^2 = 0.958) as well as a metabolism pharmacophore model (r^2 = 0.857) for the omeprazole-based series of compounds. As would be expected from the correlation of our data with lipophilic properties, both models took into account the aromaticity of the benzimidazole rings as well as multiple hydrophobic binding interactions. Interestingly, the metabolism model appeared to be more dependent on the hydrogen bond donating and accepting properties of the compounds than the inhibition model was, possibly indicating more rigid criteria for a compound to be a substrate of CYP2C19 as compared to an inhibitor of CYP2C19. In addition, substitution off of the sulfur atom appeared to affect both the metabolism and inhibition properties of the compounds in a manner more amenable to structure−activity relationships, whereas substitution at the 5-position of the benzimidazole moiety appeared to exert more influence on the observed site of metabolism.

As P450 crystal structures become more readily available, the use of docking and homology modeling has also increased and been used to predict and explore select enzyme−ligand interactions.[40−44] As the crystal structure of CYP2C19 has not been solved yet, a homology model based on the CYP2C9 crystal structure was used for active site docking studies. Two compounds were docked into the active site of CYP2C19, compounds **6** and **30**, as representatives of analogues containing an aliphatic moiety or heterocycle off of the sulfur linker. Consistent with the observed primary sites of metabolism on each molecule, the ω-1 position of compound **6** and the 5-methyl group of compound **30** were nearly superimposed approximately 3 Å from the heme iron. As both the physicochemical properties and the pharmacophore models indicated the importance of lipophilicity in predicting both the metabolism and inhibition for these compounds, it is not surprising that the closest amino acid residues to both compounds all have the potential for hydrophobic interactions. The 5-methoxy moiety of compound **6** and the pyridine nitrogen of compound **30**, which also occupied similar positions in the active site of CYP2C19, were both located within 2 Å of Ala477, indicating a potentially important role of hydrogen binding interactions with this residue in the positioning of these analogues in a catalytically favorable position within the active site of CYP2C19. Previous studies have also implicated Phe114, Ile362, and Leu 366 in the binding of hydrophobic molecules within the CYP2C19 active site.[35]

■ CONCLUSION

In summary, a highly potent set of CYP2C19 inhibitors that are also metabolized by CYP2C19 have been synthesized and used for pharmacophore and homology modeling studies with CYP2C19. Compound **30** represents the most potent CYP2C19 inhibitor currently reported in the literature. Assessing the metabolism of the compound set indicates that the primary site of metabolism is on the hydrophobic side chain off of the sulfur atom for those compounds with an aliphatic or phenyl group off of the sulfur linker and on the benzimidazole portion of the molecule for those compounds with a heterocycle adjacent to the sulfur linker. Finally, the data points to the dynamic interplay of binding affinity and metabolic stability in properly defining a K_i value for enzyme inhibitors that may also be metabolized by the same enzyme that they inhibit.

■ EXPERIMENTAL SECTION

Materials. Recombinant CYP2C19 Supersomes and 3-*O*-methylfluorescein were purchased from Becton Dickinson (San Jose, CA). NADPH was obtained from EMD Chemicals (Gibbstown, NJ). Fluorescein, magnesium sulfate, and all fine chemicals were purchased from Sigma-Aldrich (St. Louis, MO). All solvents were from J. T. Baker (Phillipsburg, NJ). Deuterated DMSO was purchased from Cambridge Isotope Laboratories (Andover, MA).

Synthesis. The appropriate mercapto-benzimidazole analogue (unsubstituted, methoxy, ethoxy, amino, methyl, or difluoromethoxy; 1.1 equiv) was dissolved in 15 mL of methanol with 3 mL of 2N sodium hydroxide and heated to 70 °C (Figure 1). Upon complete dissolution, 1 equiv of a bromo- or chloro-alkylating agent was added to the reaction and stirred at 70 °C for 12 h, at which point the reactions were checked for completion using thin layer chromatography and subsequently evaporated to dryness under a stream of nitrogen. Reactions were reconstituted in 2.5% aqueous sodium hydroxide and extracted twice with methylene chloride. The organic layers were combined, dried over magnesium sulfate, and evaporated to dryness prior to LC-MS/MS and NMR characterization. Preparative thin layer chromatography was carried out as warranted to ensure the purity of the final products (Table 1). All final products were ≥95% pure as determined by HPLC/UV/mass spectrometry.

NMR Analysis. Compounds were characterized using a 500 MHz Varian NMR spectrometer (Varian, Palo Alto, CA) using DMSO-d_6 as the solvent. Additional confirmation was obtained using electrospray ionization mass spectrometry (ESI-MS) on a ThermoFisher LTQ ion trap mass spectrometer (ThermoFisher Scientific, Waltham, MA).

Compound **1** *(115.4 mg, 47.4% yield).* δ 1.34 (t, *J* = 7.8, 3H), 3.23 (q, *J* = 5.8, 2H), 3.76 (s, 3H), 6.73 (d, *J* = 9.8, 1H), 6.97 (d, *J* = 7.8, 1H), 7.30 (dd, *J* = 5.8, 7.8, 1H), 12.34 (s, 1H). ESI-MS $(M + H)^+$ found, 209.0615; calculated for $C_{10}H_{12}N_2OS$, 209.0670.

Compound **2** *(207.5 mg, 70.5% yield).* δ 0.99 (t, *J* = 7.8, 3H), 1.70 (t, *J* = 7.8, 2H), 3.20 (m, *J* = 7.8, 2H) 3.76 (s, 3H), 6.72 (d, *J* = 7.8, 1H), 6.96 (d, *J* = 7.8, 1H), 7.31 (dd, *J* = 5.8, 7.8, 1H), 12.34 (s, 1H). ESI-MS $(M + H)^+$ found, 223.0800; calculated for $C_{11}H_{14}N_2OS$, 223.0827.

Compound **3** *(184.1 mg, 70.4% yield).* δ 0.90 (t, *J* = 7.8, 3H), 1.42 (m, *J* = 7.8, 2H), 1.67 (m, *J* = 7.8, 2H), 3.23 (t, *J* = 5.8, 2H), 3.76 (s, 3H), 6.72 (d, *J* = 7.8, 1H), 6.96 (d, *J* = 7.8, 1H), 7.32 (dd, *J* = 5.8, 7.8, 1H), 12.34 (s, 1H). ESI-MS $(M + H)^+$ found, 237.0984; calculated for $C_{12}H_{16}N_2OS$, 237.0983.

Compound **4** *(255.7 mg, 77.2% yield).* δ 0.86 (t, *J* = 7.8, 3H), 1.31 (m, *J* = 7.8, 2H), 1.38 (m, *J* = 7.8, 2H), 1.68 (m, *J* = 7.8, 2H), 3.22 (t, *J* = 7.8, 2H), 3.76 (s, 3H), 6.72 (d, *J* = 5.8, 1H), 6.94 (s, 1H), 7.30 (d, *J* = 9.8, 1H), 12.34 (s, 1H). ESI-MS $(M + H)^+$ found, 251.1196; calculated for $C_{13}H_{18}N_2OS$, 251.1140.

Compound **5** *(259.8 mg, 78.3% yield).* δ 0.86 (t, *J* = 7.3, 3H), 1.27 (m, *J* = 4.9, 4H), 1.40 (m, *J* = 7.3, 2H), 1.67 (m, *J* = 7.3, 2H), 3.22 (t, *J* = 7.3, 2H), 3.76 (s, 3H), 6.73 (d, *J* = 7.3, 1H), 6.94 (s, 1H), 7.30 (d, *J* = 9.8, 1H), 12.34 (s, 1H). ESI-MS $(M + H)^+$ found, 265.1283; calculated for $C_{14}H_{20}N_2OS$, 265.1296.

Compound **6** *(221.7 mg, 79.1% yield).* δ 0.85 (m, *J* = 12.2, 3H), 1.25 (m, *J* = 12.2, 7H), 1.39 (m, *J* = 7.3, 2H), 1.68 (m, *J* = 7.3, 2H), 3.22 (t, *J* = 7.3, 2H), 3.75 (s, 3H), 6.72 (d, *J* = 7.3, 1H), 6.94 (s, 1H), 7.31 (d, *J* = 7.3, 1H), 12.34 (s, 1H). ESI-MS $(M + H)^+$ found, 279.1466; calculated for $C_{15}H_{22}N_2OS$, 279.1453.

Compound **7** *(126.1 mg, 47.3% yield).* δ 1.00 (d, *J* = 7.8, 6H), 1.93 (m, *J* = 5.8, 1H), 3.15 (d, *J* = 3.9, 2H), 3.76 (s, 3H), 6.73 (d, *J* = 7.8, 1H), 6.92 (d, *J* = 5.8, 1H), 7.30 (dd, *J* = 7.8, 5.8, 1H), 12.50 (s, 1H). ESI-MS $(M + H)^+$ found, 237.0911; calculated for $C_{12}H_{16}N_2OS$, 237.0983.

Compound **8** *(17.1 mg, 5.7% yield).* δ 1.06 (s, 9H), 2.85 (s, 2H), 3.76 (s, 3H), 6.72 (d, *J* = 7.3, 1H), 6.94 (s, 1H), 7.31 (d, *J* = 7.3, 1H), 12.50 (s, 1H). ESI-MS $(M + H)^+$ found, 251.1127; calculated for $C_{13}H_{18}N_2OS$, 251.1140.

Compound **9** *(194.2 mg, 74.4% yield).* δ 0.31 (t, *J* = 5.8, 2H), 0.53 (t, *J* = 7.8, 2H), 1.18 (m, *J* = 3.9, 1H), 3.51 (d, *J* = 5.8, 2H), 3.76 (s, 3H), 6.73 (d, *J* = 7.8, 1H), 6.92 (d, *J* = 7.8, 1H), 7.30 (dd, *J* = 7.8, 5.8, 1H), 12.50 (s, 1H). ESI-MS $(M + H)^+$ found, 235.0868; calculated for $C_{12}H_{14}N_2OS$, 235.0827.

Compound **10** *(54.7 mg, 16.4% yield).* δ 1.01 (m, *J* = 11.7, 4H), 1.15 (m, *J* = 11.7, 2H), 1.60 (d, *J* = 7.8, 4H), 1.67 (m, *J* = 11.7, 1H), 1.83 (d, *J* = 11.7, 2H), 3.75 (s, 3H), 6.72 (d, *J* = 9.8, 1H), 6.94 (s, 1H), 7.30 (d, *J* = 9.8, 1H), 12.33 (s, 1H). ESI-MS $(M + H)^+$ found, 277.1288; calculated for $C_{15}H_{20}N_2OS$, 277.1296.

Compound **11** *(28.0 mg, 8.8% yield).* δ 1.03 (t, *J* = 5.8, 2H), 3.27 (m, *J* = 5.8, 2H), 3.51 (t, *J* = 5.8, 2H), 3.76 (s, 3H), 4.69 (t, *J* = 5.8, 1H), 6.72 (d, *J* = 9.8, 1H), 6.94 (s, 1H), 7.30 (d, *J* = 9.8, 1H), 12.33 (s, 1H). ESI-MS $(M + H)^+$ found, 239.0786; calculated for $C_{11}H_{14}N_2O_2S$, 239.0776.

Compound **12** *(32.1 mg, 10.2% yield).* δ 1.03 (t, *J* = 5.86, 2H), 3.27 (m, *J* = 5.8, 2H), 3.51 (t, *J* = 5.8, 2H), 3.76 (s, 3H), 6.72 (d, *J* = 9.8, 1H), 6.94 (s, 1H), 7.30 (d, *J* = 9.8, 1H), 10.94 (s, 1H), 12.33 (s, 1H). ESI-MS $(M + H)^+$ found, 267.0824; calculated for $C_{12}H_{14}N_2O_3S$, 267.0725.

Compound **13** *(115.2 mg, 55.3% yield).* δ 3.76 (s, 3H), 4.19 (s, 2H), 6.93 (d, *J* = 7.8, 1H), 7.10 (d, *J* = 7.8, 2H), 7.20 (s, 1H), 7.30 (m, *J* = 7.1, 2H), 7.51 (d, *J* = 7.8, 1H), 7.80 (m, J=7.8, 1H), 12.33 (s, 1H). ESI-MS $(M + H)^+$ found, 271.0865; calculated for $C_{15}H_{14}N_2OS$, 271.0827.

Compound **14** *(291.7 mg, 85.3% yield).* δ 2.25 (s, 3H), 3.76 (s, 3H), 4.47 (s, 2H), 6.74 (d, *J* = 5.8, 1H), 6.96 (s, 1H), 7.11 (d, *J* = 7.8, 2H), 7.30 (m, *J* = 5.8, 3H), 12.34 (s, 1H). ESI-MS $(M + H)^+$ found, 285.0949; calculated for $C_{16}H_{16}N_2OS$, 285.0983.

Compound **15** *(340.8 mg, 85.8% yield).* δ 1.19 (d, *J* = 5.8, 6H), 2.86 (m, *J* = 5.8, 1H), 3.76 (s, 3H), 4.19 (s, 2H), 6.72 (d, *J* = 9.8, 1H), 6.94 (s, 1H), 6.98 (m, *J* = 5.8, 2H), 7.19 (d, *J* = 5.8, 2H), 7.30 (d, *J* = 9.8, 1H), 12.33 (s, 1H). ESI-MS $(M + H)^+$ found, 313.1234; calculated for $C_{18}H_{20}N_2OS$, 313.1296.

Compound **16** *(275.6 mg, 64.1% yield).* δ 1.33 (s, 9H), 3.76 (s, 3H), 4.19 (s, 2H), 6.72 (d, *J* = 9.8, 1H), 6.94 (s, 1H), 6.98 (m, *J* = 5.8, 2H), 7.19 (d, *J* = 5.8, 2H), 7.30 (d, *J* = 9.8, 1H), 12.33 (s, 1H). ESI-MS $(M + H)^+$ found, 327.1401; calculated for $C_{19}H_{22}N_2OS$, 327.1453.

Compound **17** *(156.3 mg, 42.9% yield).* δ 3.76 (s, 3H), 4.51 (s, 2H), 6.76 (d, *J* = 5.8, 1H), 6.88 (m, *J* = 5.8, 1H), 7.10 (m, *J* = 5.8, 1H), 7.36 (d, *J* = 7.8, 2H), 7.45 (d, *J* = 9.8, 2H), 12.43 (s, 1H). ESI-MS $(M + H)^+$ found, 305.0476; calculated for $C_{15}H_{13}ClN_2OS$, 305.0437.

Compound **18** *(210.3 mg, 46.6% yield).* δ 3.76 (s, 3H), 4.51 (s, 2H), 6.74 (d, *J* = 5.8, 1H), 6.86 (m, *J* = 5.8, 1H), 7.12 (m, *J* = 5.8, 1H), 7.38 (d, *J* = 7.8, 2H), 7.47 (d, *J* = 9.8, 2H), 12.34 (s, 1H). ESI-MS $(M + H)^+$ found, 349.0092; calculated for $C_{15}H_{13}BrN_2OS$, 348.9932.

Compound **19** *(365.9 mg, 78.5% yield).* δ 3.76 (s, 3H), 4.47 (s, 2H), 6.65 (d, *J* = 11.7, 1H), 6.95 (m, *J* = 7.8, 1H), 7.23 (d, *J* = 7.8, 2H), 7.33 (m, *J* = 7.8, 1H), 7.66 (d, *J* = 7.8, 2H), 12.43 (s, 1H). ESI-MS $(M + H)^+$ found, 396.9782; calculated for $C_{15}H_{13}IN_2OS$, 396.9793.

Compound **20** *(36.4 mg, 12.5% yield).* δ 3.87 (s, 3H), 4.19 (s, 2H), 6.65 (d, *J* = 11.7, 1H), 6.95 (m, *J* = 7.8, 1H), 7.23 (d, *J* = 7.8, 2H), 7.33 (m, *J* = 7.8, 1H), 7.66 (d, *J* = 7.8, 2H), 12.58 (s, 1H), 12.78 (s, 1H). ESI-MS $(M + H)^+$ found, 315.0752; calculated for $C_{16}H_{14}N_2O_3S$, 315.0725.

Compound **21** *(230.7 mg, 59.5% yield).* δ 3.63 (s, 6H), 3.76 (s, 3H), 4.19 (s, 2H), 6.13 (s, 2H), 6.18 (s, 1H) 6.72 (d, *J* = 9.8, 1H), 6.94 (s, 1H), 7.30 (d, *J* = 9.8, 1H), 12.34 (s, 1H). ESI-MS $(M + H)^+$ found, 331.0888; calculated for $C_{17}H_{18}N_2O_3S$, 331.1038.

Compound **22** *(296.2 mg, 70.8% yield).* δ 3.75 (s, 3H), 4.45 (s, 2H), 6.73 (d, *J* = 5.8, 1H), 6.93 (m, *J* = 5.8, 1H), 7.25 (d, *J* = 5.8, 1H), 7.30 (m, *J* = 9.8, 1H), 7.37 (m, *J* = 5.8, 2H), 7.42 (m, *J* = 5.8, 2H), 7.46 (m, *J* = 5.8, 2H), 7.60 (d, *J* = 5.8, 1H), 12.36 (s, 1H). ESI-MS $(M + H)^+$ found, 347.0996; calculated for $C_{21}H_{18}N_2OS$, 347.1140.

Compound **23** *(194.1 mg, 57.0% yield).* δ 3.76 (s, 3H), 4.50 (s, 2H), 6.94 (d, *J* = 7.8, 1H), 7.12 (s, 1H), 7.18 (d, 1H), 7.55 (m, *J* = 7.8, 6H), 8.02 (d, *J* = 5.8, 1H), 12.33 (s, 1H). ESI-MS $(M + H)^+$ found, 321.0957; calculated for $C_{19}H_{16}N_2OS$, 321.0983.

Compound **24** *(175.4 mg, 67.2% yield).* δ 3.76 (s, 3H), 4.56 (s, 2H), 6.72 (d, *J* = 9.8, 1H), 6.94 (s, 1H), 7.30 (m, *J* = 9.8, 2H), 7.54 (t, *J* = 7.8, 1H), 7.73 (t, *J* = 7.8, 1H), 7.94 (m, *J* = 5.8, 2H), 8.02 (d, *J* = 5.8, 1H), 12.33 (s, 1H). ESI-MS $(M + H)^+$ found, 322.1072; calculated for $C_{18}H_{15}N_3OS$, 322.0936.

Compound **25** *(428.6 mg, 91.0% yield).* δ 3.76 (s, 3H), 4.50 (d, *J* = 11.7, 2H), 6.74 (d, *J* = 5.8, 1H), 6.87 (d, *J* = 7.8, 1H), 6.95 (d, *J* = 7.8, 2H), 7.07 (d, *J* = 9.8, 1H), 7.12 (t, *J* = 7.7, 1H), 7.19 (d, *J* = 5.8, 1H), 7.23 (d, *J* = 7.8, 1H), 7.31 (m, *J* = 7.8, 1H), 7.38 (d, *J* = 7.8, 3H), 12.34 (s, 1H). ESI-MS $(M + H)^+$ found, 363.1063; calculated for $C_{21}H_{18}N_2O_2S$, 363.1089.

Compound **26** *(403.1 mg, 80.5% yield).* δ 3.76 (s, 3H), 4.29 (s, 2H), 5.14 (s, 2H), 6.65 (d, *J* = 7.8, 2H), 6.87 (d, *J* = 7.8, 2H), 6.72 (d, *J* = 9.8, 1H), 6.94 (s, 1H), 7.30 (d, *J* = 9.8, 1H), 7.37 (t, *J* = 7.8, 1H), 7.41 (t, *J* = 5.8, 2H), 7.48 (d, *J* = 5.8, 2H), 12.43 (s, 1H). ESI-MS $(M + H)^+$ found, 376.9986; calculated for $C_{22}H_{20}N_2O_2S$, 377.1245.

Compound **27** *(114.2 mg, 57.6% yield).* δ 3.76 (s, 3H), 4.51 (s, 2H), 6.93 (d, *J* = 7.8, 1H), 7.12 (s, 1H), 7.15 (t, *J* = 7.8, 1H), 7.30 (d, *J* = 9.8, 1H), 7.56 (d, *J* = 7.8, 1H), 7.74 (t, *J* = 7.8, 1H), 8.67 (d, *J* = 7.8, 1H), 12.43 (s, 1H). ESI-MS $(M + H)^+$ found, 272.0748; calculated for $C_{14}H_{13}N_3OS$, 272.0779.

Compound **28** *(132.2 mg, 64.2% yield).* δ 1.33 (t, *J* = 7.8, 3H), 4.01 (m, *J* = 7.8, 2H), 4.63 (d, *J* = 11.7, 2H), 6.74 (t, *J* = 7.8, 1H), 6.87 (s, 1H), 7.27 (m, *J* = 3.8, 1H), 7.39 (d, *J* = 7.8, 1H), 7.51 (t, *J* = 7.8, 1H), 7.78 (t, *J* = 7.8, 1H), 8.51 (d, *J* = 3.9, 1H), 12.47 (s, 1H). ESI-MS $(M + H)^+$ found, 286.0978; calculated for $C_{15}H_{15}N_3OS$, 286.0936.

Compound **29** *(146.3 mg, 66.4% yield).* δ 4.52 (s, 2H), 7.15 (t, *J* = 9.8, 1H), 7.21 (t, *J* = 7.8, 2H), 7.27 (d, *J* = 9.8, 1H), 7.45 (d, *J* = 7.8, 2H), 7.74 (t, *J* = 7.8, 1H), 8.67 (d, *J* = 7.8, 1H), 12.43 (s, 1H). ESI-MS $(M + H)^+$ found, 242.0643; calculated for $C_{13}H_{11}N_3S$, 242.0674.

Compound **30** *(283.9 mg, 86.7% yield).* δ 2.38 (s, 3H), 4.65 (s, 2H), 6.91 (s, 1H), 6.96 (d, *J* = 8.8, 1H), 7.29 (m, *J* = 5.8, 2H), 7.51 (d, *J* = 8.8, 1H), 7.75 (t, *J* = 8.8, 1H), 8.52 (d, *J* = 5.8, 1H),

dx.doi.org/10.1021/jm201346g | *J. Med. Chem.* 2012, 55, 1205−1214

12.33 (s, 1H). ESI-MS $(M + H)^+$ found, 256.0803; calculated for $C_{14}H_{13}N_3S$, 256.0830.

Compound ***31*** *(292.3 mg, 74.4% yield).* δ 4.67 (s, 2H), 6.97 (d, J = 9.8, 1H), 7.02 (s, 1H), 7.17 (s, 1H), 7.24 (t, J = 72.6, 1H), 7.30 (m, J = 3.9, 1H), 7.40 (d, J = 7.8, 1H), 7.53 (d, J = 7.8, 1H), 8.52 (d, J = 5.8, 1H), 12.33 (s, 1H). ESI-MS $(M + H)^+$ found, 308.0608; calculated for $C_{14}H_{11}F_2N_3OS$, 308.0591.

Compound ***32*** *(75.6 mg, 32.5% yield).* δ 4.52 (s, 2H), 5.85 (s, 2H), 6.72 (d, J = 9.8, 1H), 6.94 (s, 1H), 7.15 (t, J = 7.8, 1H), 7.27 (d, J = 7.8, 1H), 7.30 (d, J = 9.8, 1H), 7.74 (t, J = 7.8, 1H), 8.67 (d, J = 7.8, 1H), 12.43 (s, 1H). ESI-MS $(M + H)^+$ found, 257.0792; calculated for $C_{13}H_{12}N_4S$, 257.0783.

P450 Inhibition Assay. Inhibition of recombinant CYP2C19 microsomes was determined for each analogue using 3-*O*-methylfluorescein as a probe substrate. Initial experiments were performed to ensure reaction linearity with respect to protein and time. Each incubation (n = 2) consisted of 2 pmol recombinant protein in 100 mM potassium phosphate buffer (pH 7.4) containing 3 mM $MgCl_2$. Following a 3 min preincubation period, reactions were initiated with the addition of 1 mM NADPH (final concentration). Organic solvent concentrations were the same for all incubations and did not exceed 0.5% (v/v). IC_{50} values for each analogue were determined for CYP2C19 using a final test compound concentration range of 0−50 μM. 3-*O*-methylfluorescein was run at 1 μM (approximate K_m). All incubations were allowed to proceed at 37 °C for 5 min and quenched with 50 μL of 2N NaOH. Samples were vortex-mixed for 5 min prior to analysis.

Once IC_{50} values were estimated, a K_i was determined for each test compound against CYP2C19 catalyzed 3-*O*-methylfluorescein metabolism. K_i experiments were run under similar conditions as the IC_{50} determination except that the probe substrate was run at 0.5, 1, 2, and 4 μM corresponding to concentrations equal to 0.5 K_m, K_m, 2K_m, and 4K_m, respectively. Each test compound was run at 0IC_{50}, 0.5IC_{50}, IC_{50}, 2IC_{50}, and 4IC_{50}. Incubations were allowed to proceed at 37 °C for 5 min and quenched with 50 μL of 2N NaOH. All K_i determinations were performed in duplicate.

Sample analysis was performed on a Tecan Safire^2 microplate reader (Männedorf, Switzerland). Fluorescein formation was monitored using an excitation wavelength of 485 nm (10 nm bandwidth) and an emission wavelength of 530 nm (20 nm bandwidth). A manual gain of 40 (arbitrary units) was utilized with no lag time and an integration time of 40 μs. Each sample was read twice and the average response used in IC_{50} and K_i calculations.

To determine the selectivity of the omeprazole analogues versus other P450 isoforms, IC_{50} determinations were carried out in human liver microsomes with P450-selective substrate probes. Briefly, 0.1 mg/mL human liver microsomes, 3 mM $MgCl_2$, 100 mM potassium phosphate buffer (pH 7.4), and the P450-selective substrate probe at previously determined K_m value (CYP1A2, 85 μM phenacetin; CYP2B6, 75 μM bupropion; CYP2C8, 7 μM paclitaxel; CYP2C9, 17 μM diclofenac; CYP2C19, 10 μM (*S*)-mephenytoin; CYP2D6, 5 μM dextromethorphan; CYP2E1, 75 μM chlorzoxazone; CYP3A4, 2.5 μM midazolam) were combined with each omeprazole analogue (0−50 μM, final concentration) and preincubated for 5 min at 37 °C. Reactions were initiated via addition of 1 mM NADPH (final concentration) and quenched after 10 min (5 min for midazolam) with 2 volumes of ice cold acetonitrile containing 1 μM tolbutamide as an internal standard.

LC-MS/MS analysis for the inhibition assay was carried out using multiple reaction monitoring on an Applied Biosystems API 4000 Q-Trap (operated in triple quadrupole mode) equipped with an electrospray ionization source (Applied Biosystems, Foster City, CA). Prior to analysis, mass spectrometry parameters were optimized for each test compound. Global mass spectrometry settings included the curtain gas (40 arbitrary units), ion spray voltage (4700 V), source temperature (550 °C), and collision-assisted dissociation gas (set to medium). Chromatographic separation was achieved using a rapid gradient with a Gemini C18 30 mm × 2.0 mm (5 μm) column (Phenomenex, Torrace, CA) coupled to two LC-20AD pumps with an in-line CBM-20A controller and DGU-20A_5 solvent degasser (Shimadzu, Columbia, MD) and a LEAP CTC HTS PAL autosampler equipped with a dual-solvent self-washing system (CTC Analytics, Carrboro, NC).

Statistical Analysis. Inhibition data (IC_{50} and K_i) was calculated using Graphpad Prism (version 5.01; Graphpad Software Inc., San Diego, CA). For fluorescence assays, all parameters were calculated after first subtracting out background fluorescence from 3-*O*-methylfluorescein. Inhibition curves were fit to a standard four-site eq 1 to estimate an IC_{50} value.

$$\%\text{activity} = \min + \frac{(\max - \min)}{(1 + 10^{(\log[I] - \log IC_{50})})} \quad (1)$$

K_i estimates were determined using nonlinear regression analysis. The mechanism of inhibition and inhibitory model selection was determined through visual inspection of the Dixon ($[I]$ vs $1/v$) and Lineweaver−Burke ($1/S$ vs $1/v$) plots and through comparison of the Akaike information criteria. All data were subsequently fit to a competitive inhibition model (2), where $[S]$ is the probe substrate concentration, K_m is equal to the probe substrate concentration at half-maximum reaction velocity, $[I]$ is the test compound concentration in the incubation, and K_i is the dissociation constant for the enzyme−inhibitor complex. For K_i determinations, K_m, K_i, and V_{max} were treated as global parameters. Goodness of fit was determined using global r^2 values.

$$v = \frac{V_{max} \cdot [S]}{K_m\left(1 + \frac{[I]}{K_i}\right) + [S]} \quad (2)$$

Intrinsic Clearance Determination. To support the generation of a pharmacophore model and assess the stability of the omeprazole analogues, intrinsic clearance determinations were carried out in recombinant CYP2C19 and human liver microsomes. Incubations in recombinant CYP2C19 included 2 pmol CYP2C19, 2 mM $MgCl_2$, and 0.5 μM substrate in 100 mM potassium phosphate buffer (pH 7.4). Incubations were initiated with the addition of 1 mM NADPH (final concentration) and aliquots removed at 0, 2.5, 5, 10, 20, and 40 min. Reactions were quenched with 1 volume (v/v) of ice-cold acetonitrile containing 1 μM tolbutamide as an internal standard. Human liver microsomal clearance determinations were carried out in a similar fashion and contained 0.1 mg/mL human liver microsomes, 3 mM $MgCl_2$, and 0.5 μM substrate in 100 mM potassium phosphate buffer (pH 7.4). LC-MS/MS analysis of the omeprazole analogues was performed using a similar instrumental protocol to that described for the CYP inhibition assays.

Pharmacophore Model Generation. Ligands (compounds **1** through **26**) were prepared using LigPrep (Ligprep 2.0 (2006) Schrodinger, LLC, New York, NY), which attached hydrogen atoms and converted two-dimensional .sdf files to three-dimensional structures with proper stereocenters. The ligands were generated as a neutral series. Ligand conformations were submitted to a pre-energy minimization using the OPLS_2005 force field with a distance dependent dielectric model. A maximum of 200 initial conformers were examined. Minimized structures within 1 kcal energy and rmsd of 1 Å or less were eliminated. Each ligand was examined against the six default pharmacophore features: hydrogen bond acceptor (A), hydrogen bond donor (D), hydrophobic (H), negative charge (N), positive ionization (P), and aromatic ring (R). The pharmacophore model was generated using feature-based pharmacophore model. Four ligands were chosen as active ligands for the model. Active compounds were chosen based upon two criteria: (1) active compounds must reside within the top 15% with respect to inhibitor potency and (2) must contain some sense of structural diversity from one another. The number of pharmacophore features was varied from a minimum of three to a maximum of six features during the alignment process with a limit of three hydrophobic sites allowed. Common pharmacophores features were required to match at least 3 of the 4 active compounds. Upon the basis of the size of pharmacophore set, a maximum of three principal features were allowed. During pharmacophore hypothesis testing, 50% of ligands were randomly assigned to the training set,

while the remainder was included as the test set. The remaining model criteria were set to PHASE default parameters.

Metabolite Identification in rCYP2C19. To elucidate the sites of metabolism of the omeprazole analogues, metabolite identification studies were performed in recombinant CYP2C19. Briefly, incubations contained 20 pmol CYP2C19, 3 mM $MgCl_2$, and 20 μM substrate in 100 mM potassium phosphate buffer (pH 7.4). Incubations were allowed to proceed for 20 min before being quenched with 2 volumes of ice-cold acetonitrile containing 0.1% formic acid (v/v). Samples were centrifuged, and the resulting supernatant collected and evaporated under nitrogen. Prior to mass spectral/UV analysis, samples were reconstituted in water:acetonitrile:formic acid (50:50:0.1). Analysis of metabolite formation was performed on a ThermoFisher LTQ ion trap mass spectrometer. Chromatographic separation was achieved using a Luna C18 150 μm × 2.0 5 μm column (Phenomenex, Torrance, CA) and a 20 min linear gradient from 95:5 A:B to 5:95 A:B (A, water containing 0.1% formic acid; B, acetonitrile containing 0.1% formic acid) at a flow rate of 250 μL/min.

CYP2C19 Homology Model Studies. A three-dimensional homology model of CYP2C19 was built using Prime (Schrodinger, LLC, New York, NY) and was based on the crystal structure of CYP2C9 with flurbiprofen bound (PDB file 1R9O). The crystal structure of CYP2C9 was chosen due to its sequence homology with CYP2C19 and because it did not contain any amino acid modifications. The amino acid sequence of CYP2C19 was obtained from GenBank (CAH73444.1). Ramachandran plots confirmed the structural plausibility of the homology model. Visual evaluation of the model detected no odd bond angles or bond lengths.

SiteMap (Schrodinger, LLC) located and defined the P450 2C19 active site using a series of adjacent dummy atoms that estimated the size and boundary of the active site. The SiteMap-defined active site was employed to generate the docking grid for subsequent docking experiments. The docking grid was defined by a 14 × 14 × 14 $Å^3$ box whereby the mass center of the each docked ligand was centered. The remaining algorithm parameters were set to the default settings. Ligands were docked using the Ligand Docking algorithm within Glide (Schrodinger, LLC). Individual ligand poses were examined either by GlideScore or eModel. Prior to docking, ligands were prepared in a similar fashion to that described for the pharmacophore model.

AUTHOR INFORMATION

Corresponding Author

*Phone: 206-265-7423. E-mail: janw@amgen.com.

Notes

The authors declare no competing financial interest.

ACKNOWLEDGMENTS

We acknowledge Dr. Brooke M. VandenBrink for valuable assistance in preparing the pharmacophore and homology model figures.

ABBREVIATIONS USED

P450, cytochrome P450; QSAR, quantitative structure−activity relationship; K_i, inhibition constant; Cl_{int}, intrinsic clearance; LC-MS/MS, liquid chromatography-tandem mass spectrometry

REFERENCES

(1) Ortiz de Montellano, P. R.; De Voss, J. J. Substrate Oxidation by Cytochrome P450 Enzymes. In *Cytochrome P450: Structure, Mechanism, and Biochemistry*, 3rd ed.; Ortiz de Montellano, P. R., Ed.; Kluwer Academic/Plenum Publishers: New York, 2005; pp 183−245.

(2) Guengerich, F. P. Human Cytochrome P450 Enzymes. In *Cytochrome P450: Structure, Mechanism, and Biochemistry*, 3rd ed.; Ortiz de Montellano, P. R., Ed.; Kluwer Academic/Plenum Publishers: New York, 2005; pp 377−530.

(3) Guengerich, F. P.; MacDonald, J. S. Applying mechanisms of chemical toxicity to predict drug safety. *Chem. Res. Toxicol.* **2007**, *20*, 344−369.

(4) Denton, T. T.; Zhang, X.; Cashman, J. R. 5-Substituted, 6-Substituted, and Unsubstituted 3-Heteroaromatic Pyridine Analogues of Nicotine as Selective Inhibitors of Cytochrome P-450 2A6. *J. Med. Chem.* **2004**, *48*, 224−239.

(5) Gomaa, M. S.; Bridgens, C. E.; Aboraia, A. S.; Veal, G. J.; Redfern, C. P.; Brancale, A.; Armstrong, J. L.; Simons, C. Small Molecule Inhibitors of Retinoic Acid 4-Hydroxylase (CYP26): Synthesis and Biological Evaluation of Imidazole Methyl 3-(4-(Aryl-2-ylamino)-phenyl)propanoates. *J. Med. Chem.* **2011**, *54*, 6803−6811.

(6) Kim, S.; Ko, H.; Park, J. E.; Jung, S.; Lee, S. K.; Chun, Y.-J. Design, Synthesis, and Discovery of Novel *trans*-Stilbene Analogues as Potent and Selective Human Cytochrome P450 1B1 Inhibitors. *J. Med. Chem.* **2001**, *45*, 160−164.

(7) Paine, M. F.; Hart, H. L.; Ludington, S. S.; Haining, R. L.; Rettie, A. E.; Zeldin, D. C. The human intestinal cytochrome P450 "pie". *Drug Metab. Dispos.* **2006**, *34*, 880−886.

(8) Ring, B. J.; Eckstein, J. A.; Gillespie, J. S.; Binkley, S. N.; VandenBranden, M.; Wrighton, S. A. Identification of the human cytochromes p450 responsible for in vitro formation of *R*- and *S*-norfluoxetine. *J. Pharmacol. Exp. Ther.* **2001**, *297*, 1044−1050.

(9) Feng, H. J.; Huang, S. L.; Wang, W.; Zhou, H. H. The induction effect of rifampicin on activity of mephenytoin 4′-hydroxylase related to M1 mutation of CYP2C19 and gene dose. *Br. J. Clin. Pharmacol.* **1998**, *45*, 27−29.

(10) Raucy, J. L.; Mueller, L.; Duan, K.; Allen, S. W.; Strom, S.; Lasker, J. M. Expression and induction of CYP2C P450 enzymes in primary cultures of human hepatocytes. *J. Pharmacol. Exp. Ther.* **2002**, *302*, 475−482.

(11) Foti, R. S.; Wahlstrom, J. L. CYP2C19 inhibition: the impact of substrate probe selection on in vitro inhibition profiles. *Drug Metab. Dispos.* **2008**, *36*, 523−528.

(12) Wang, J. H.; Li, P. Q.; Fu, Q. Y.; Li, Q. X.; Cai, W. W. Cyp2c19 genotype and omeprazole hydroxylation phenotype in Chinese Li population. *Clin. Exp. Pharmacol. Physiol.* **2007**, *34*, 421−424.

(13) Holt, S.; Howden, C. W. Omeprazole. Overview and opinion. *Digestive Dis. Sci.* **1991**, *36*, 385−393.

(14) Howden, C. W. Clinical pharmacology of omeprazole. *Clin. Pharm.* **1991**, *20*, 38−49.

(15) Spencer, C. M.; Faulds, D. Lansoprazole. A reappraisal of its pharmacodynamic and pharmacokinetic properties, and its therapeutic efficacy in acid-related disorders. *Drugs* **1994**, *48*, 404−430.

(16) Meyer, U. A. Metabolic interactions of the proton-pump inhibitors lansoprazole, omeprazole and pantoprazole with other drugs. *Eur. J. Gastroenterol. Hepatol.* **1996**, *8* (Suppl 1), S21−S25.

(17) Meyer, U. A. Interaction of proton pump inhibitors with cytochromes P450: consequences for drug interactions. *Yale J. biol. Med.* **1996**, *69*, 203−209.

(18) Ko, J. W.; Sukhova, N.; Thacker, D.; Chen, P.; Flockhart, D. A. Evaluation of omeprazole and lansoprazole as inhibitors of cytochrome P450 isoforms. *Drug Metab. Dispos.* **1997**, *25*, 853−862.

(19) Andersson, T.; Andren, K.; Cederberg, C.; Edvardsson, G.; Heggelund, A.; Lundborg, P. Effect of omeprazole and cimetidine on plasma diazepam levels. *Eur. J. Clin. Pharmacol.* **1990**, *39*, 51−54.

(20) Andersson, T.; Cederberg, C.; Edvardsson, G.; Heggelund, A.; Lundborg, P. Effect of omeprazole treatment on diazepam plasma levels in slow versus normal rapid metabolizers of omeprazole. *Clin. Pharmacol. Ther.* **1990**, *47*, 79−85.

(21) Enderle, C.; Muller, W.; Grass, U. Drug interaction: omeprazole and phenprocoumon. *BMC Gastroenterol.* **2001**, *1*, 2.

(22) Pearson, J.; Dahal, U. P.; Rock, D.; Peng, C. C.; Schenk, J. O.; Joswig-Jones, C.; Jones, J. P. The kinetic mechanism for cytochrome P450 metabolism of type II binding compounds: evidence supporting direct reduction. *Arch. Biochem. Biophys.* **2011**, *511*, 69−79.

(23) Peng, C. C.; Pearson, J. T.; Rock, D. A.; Joswig-Jones, C. A.; Jones, J. P. The effects of type II binding on metabolic stability and

binding affinity in cytochrome P450 CYP3A4. *Arch. Biochem. Biophys.* **2010**, *497*, 68−81.
(24) Chiba, M.; Jin, L.; Neway, W.; Vacca, J. P.; Tata, J. R.; Chapman, K.; Lin, J. H. P450 interaction with HIV protease inhibitors: relationship between metabolic stability, inhibitory potency, and P450 binding spectra. *Drug Metab. Dispos.* **2001**, *29*, 1−3.
(25) Li, H.; Sun, J.; Fan, X.; Sui, X.; Zhang, L.; Wang, Y.; He, Z. Considerations and recent advances in QSAR models for cytochrome P450-mediated drug metabolism prediction. *J. Comput.-Aided Mol. Des.* **2008**, *22*, 843−855.
(26) Locuson, C. W. II; Suzuki, H.; Rettie, A. E.; Jones, J. P. Charge and substituent effects on affinity and metabolism of benzbromarone-based CYP2C19 inhibitors. *J. Med. Chem.* **2004**, *47*, 6768−6776.
(27) Ridderstrom, M.; Zamora, I.; Fjellstrom, O.; Andersson, T. B. Analysis of selective regions in the active sites of human cytochromes P450, 2C8, 2C9, 2C18, and 2C19 homology models using GRID/CPCA. *J. Med. Chem.* **2001**, *44*, 4072−4081.
(28) Yao, Y.; Han, W. W.; Zhou, Y. H.; Li, Z. S.; Li, Q.; Chen, X. Y.; Zhong, D. F. The metabolism of CYP2C9 and CYP2C19 for gliclazide by homology modeling and docking study. *Eur. J. Med. Chem.* **2009**, *44*, 854−861.
(29) Suzuki, H.; Kneller, M. B.; Haining, R. L.; Trager, W. F.; Rettie, A. E. (+)-*N*-3-Benzyl-nirvanol and (−)-*N*-3-Benzyl-phenobarbital: new potent and selective in vitro inhibitors of CYP2C19. *Drug Metab. Dispos.* **2002**, *30*, 235−239.
(30) Houston, J. B., Kenworthy, K. E. Galetin, A. Typical and Atypical Enzyme Kinetics. In *Drug Metabolizing Enzymes: Cytochrome P450 and Other Enzymes in Drug Discovery and Development*; Lee, J. S., Obach, R. S., Fisher, M. B., Eds.; Marcel Dekker: New York, 2003; pp 211−254.
(31) Sutton, D.; Butler, A. M.; Nadin, L.; Murray, M. Role of CYP3A4 in human hepatic diltiazem *N*-demethylation: inhibition of CYP3A4 activity by oxidized diltiazem metabolites. *J. Pharmacol. Exp. Ther.* **1997**, *282*, 294−300.
(32) Fukushima, Y.; Ushimaru, M.; Takahara, S. On the error of the dixon plot for estimating the inhibition constant between enzyme and inhibitor. *Biochem. Mol. Biol. Ed.* **2002**, *30*, 90−92.
(33) Carter, C. M.; Leighton-Davies, J. R.; Charlton, S. J. Miniaturized receptor binding assays: complications arising from ligand depletion. *J. Biomol. Screening* **2007**, *12*, 255−266.
(34) Lewis, D. F.; Lake, B. G.; Ito, Y.; Dickins, M. Lipophilicity relationships in inhibitors of CYP2C9 and CYP2C19 enzymes. *J. Enzyme Inhib. Med. Chem.* **2006**, *21*, 385−389.
(35) Suzuki, H.; Kneller, M. B.; Rock, D. A.; Jones, J. P.; Trager, W. F.; Rettie, A. E. Active-site characteristics of CYP2C19 and CYP2C9 probed with hydantoin and barbiturate inhibitors. *Arch. Biochem. Biophys.* **2004**, *429*, 1−15.
(36) Ekins, S.; Bravi, G.; Binkley, S.; Gillespie, J. S.; Ring, B. J.; Wikel, J. H.; Wrighton, S. A. Three and four dimensional-quantitative structure−activity relationship (3D/4D-QSAR) analyses of CYP2D6 inhibitors. *Pharmacogenetics* **1999**, *9*, 477−489.
(37) Ekins, S.; Bravi, G.; Binkley, S.; Gillespie, J. S.; Ring, B. J.; Wikel, J. H.; Wrighton, S. A. Three- and four-dimensional quantitative structure−activity relationship analyses of cytochrome P-450 3A4 inhibitors. *J. Pharmacol. Exp. Ther.* **1999**, *290*, 429−438.
(38) Ekins, S.; de Groot, M. J.; Jones, J. P. Pharmacophore and three-dimensional quantitative structure−activity relationship methods for modeling cytochrome p450 active sites. *Drug Metab. Dispos.* **2001**, *29*, 936−944.
(39) Sciabola, S.; Morao, I.; de Groot, M. J. Pharmacophoric fingerprint method (TOPP) for 3D-QSAR modeling: application to CYP2D6 metabolic stability. *J. Chem. Inf. Model.* **2007**, *47*, 76−84.
(40) Rowland, P.; Blaney, F. E.; Smyth, M. G.; Jones, J. J.; Leydon, V. R.; Oxbrow, A. K.; Lewis, C. J.; Tennant, M. G.; Modi, S.; Eggleston, D. S.; Chenery, R. J.; Bridges, A. M. Crystal structure of human cytochrome P450 2D6. *J. Biol. Chem.* **2006**, *281*, 7614−7622.
(41) Schoch, G. A.; Yano, J. K.; Wester, M. R.; Griffin, K. J.; Stout, C. D.; Johnson, E. F. Structure of human microsomal cytochrome P450 2C8. Evidence for a peripheral fatty acid binding site. *J. Biol. Chem.* **2004**, *279*, 9497−9503.
(42) Wester, M. R.; Yano, J. K.; Schoch, G. A.; Yang, C.; Griffin, K. J.; Stout, C. D.; Johnson, E. F. The structure of human cytochrome P450 2C9 complexed with flurbiprofen at 2.0-A resolution. *J. Biol. Chem.* **2004**, *279*, 35630−35637.
(43) Williams, P. A.; Cosme, J.; Ward, A.; Angove, H. C.; Matak Vinkovic, D.; Jhoti, H. Crystal structure of human cytochrome P450 2C9 with bound warfarin. *Nature* **2003**, *424*, 464−468.
(44) Yano, J. K.; Wester, M. R.; Schoch, G. A.; Griffin, K. J.; Stout, C. D.; Johnson, E. F. The structure of human microsomal cytochrome P450 3A4 determined by X-ray crystallography to 2.05-A resolution. *J. Biol. Chem.* **2004**, *279*, 38091−38094.